JOURNAL OF CATALYSIS 157, 472–481 (1995)

Observation of Molecular Reaction Intermediate and Reaction Mechanism for NO Dissociation and NO–H_2 Reaction on Rh–Sn/SiO_2 Catalysts

Keiichi Tomishige,[1] Kiyotaka Asakura, and Yasuhiro Iwasawa[2]

Department of Chemistry, Graduate School of Science, The University of Tokyo, Hongo, Bunkyo-ku, Tokyo 113, Japan

Received August 22, 1994; revised July 10, 1995; accepted July 20, 1995

The Rh–Sn/SiO_2 catalyst prepared by the selective reaction between Sn $(CH_3)_4$ vapor and Rh particles on SiO_2 was remarkably active for the NO dissociation and the catalytic NO–H_2 reaction. To obtain structural information on the behavior of molecularly adsorbed intermediates related to the high activity of the bimetallic ensemble catalyst surface, *in situ* EXAFS and FTIR were employed, in parallel with reaction kinetics. We observed the molecular reaction intermediate, bent-type NO, by EXAFS with the aid of FTIR. The reaction mechanism is discussed on the basis of the characterization of adsorbed species and surface bimetallic structure. © 1995 Academic Press, Inc.

INTRODUCTION

The aim of this study is to observe directly the intermediate NO species of catalytic NO–H_2 reaction and to explore the reaction mechanism on Rh–Sn/SiO_2 catalysts by EXAFS, FTIR, and reaction kinetics.

Recently we found that the Rh–Sn/SiO_2 catalysts prepared by the reaction of Sn $(CH_3)_4$ with Rh/SiO_2 have a much higher activity for NO dissociation and catalytic NO–H_2 reaction than a monometallic Rh/SiO_2 catalyst and a coimpregnation Rh–Sn/SiO_2 catalyst (1). The active bimetallic ensemble structure has been characterized by means of Sn *k*-edge and Rh *K*-edge EXAFS, TEM, FTIR, and CO and H_2 adsorptions (2, 3). It was suggested that Sn atoms in Rh–Sn/SiO_2 were located at the first layer of the particles in the range of Sn/Rh $\leqq$ 0.4 to reach the saturation coverage (Sn/Rh = 0.4), showing the surface composition Sn_s/Rh_s of three, where a Rh atom is surrounded by six Sn atoms on the assumption of *fcc*(111) bimetallic surface as shown in Fig. 1 (2, 3). In addition, the distance between the first layer and the second layer of the bimetallic particles was found to become longer by 0.024 nm than the distance in Rh *fcc* metal as a result of the relaxation of surface structure (3). The active bimetallic surface at Sn_s/Rh_s = 3 may be a good sample prepared by a molecular level strategy (1–3).

The strategy for the design of bimetallic surface structures on SiO_2, active for the catalytic NO–H_2 reaction, was to create bimetallic ensemble sites composed of Rh and Sn as an oxophilic metal. In the ensemble sites of Fig. 1, Sn atoms can interact with the oxygen atom of NO molecule adsorbed on Rh atom to weaken the N–O bond for its dissociation, which may be enhanced by the larger size of the Sn atom than the Rh atom, because the oxygen atom of NO adsorbed on a Rh atom is closer to the surrounding Sn atoms protruded slightly in the geometry. The resultant Sn–O bonds can be readily reduced cleaved by hydrogen to restore the original metallic state of stain (4). The oxophilic character of the Sn atom has been reported for CO oxidation reaction on Rh–Sn/SiO_2. It has been claimed that Sn enhanced the activation of the oxygen molecule, decreased the self-poisoning by CO and/or O_2, and promoted the surface reaction between adsorbed oxygen and weakly adsorbed CO (5). In selective hydrogenolysis for ethylacetate into ethanol on Rh–Sn/SiO_2, Ru–Sn/SiO_2, Ni–Sn/SiO_2, the selectivity to ethanol was much higher than that for the corresponding monometallic catalysts, where the Sn atom was suggested to interact with the oxygen lone pair of the carbonyl group of ethylacetate (6–9).

The removal of NO in exhaust gases by converting it to N_2 and N_2O is an important subject from environmental points of view. In the NO–H_2 reaction and the NO–CO reaction on noble metals like Pt and Rh, the rate-determining step has been demonstrated to be a NO dissociation (10, 11). It is important to promote NO dissociation for enhancement of NO reduction on these metals, whereas additive Sn atoms remarkably enhanced both the NO dissociation and the catalytic NO–H_2 reaction.

Direct observation of reaction intermediate for NO–H_2 reaction on Rh–Sn/SiO_2 by means of EXAFS has been recently reported in a short communication (12). In this

[1] Current address: Department of Applied Chemistry, Faculty of Engineering, The University of Tokyo, Hongo, Bunkyo-ku, Tokyo 113

[2] To whom correspondence should be addressed.

0021-9517/95 $12.00

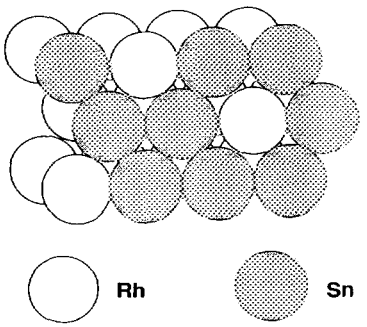

FIG. 1. A surface model structure (top view) of Rh–Sn/SiO_2 (Sn/Rh = 0.4) assuming that Rh–Sn bimetallic particles are spherical and have a *fcc*(111) surface.

article, we report the structural and chemical activation of adsorbed NO molecules by Sn atoms and the reaction mechanism for the NO–H_2 reaction promoted by Sn atoms in relation to so-called promoter effects by means of *in situ* EXAFS at the Sn *K*-edge and FTIR with the aid of reaction kinetics.

EXPERIMENTAL

Preparation of Catalysts

SiO_2 (Aerosil 200:200 m^2/g) was impregnated with a methanol solution of $RhCl_3 \cdot 3H_2O$ (Soekawa Chemical Co.), followed by drying at 373 K for 12 h and reduction with H_2 at 573 K for 1 h. The obtained Rh particles on SiO_2 were then reacted with a given amount of $Sn(Ch_3)_4$ (Soekawa Chemical Co.) vapor (<0.6 kPa) at 423 K for 15 min in a closed circulating system (dead volume, 200 cm^3). At this temperature the decomposition of $Sn(CH_3)_4$ on Rh metal surfaces took place much more rapidly than the reaction of $Sn(CH_3)_4$ and OH groups of SiO_2. Under the present conditions nearly 100% of $Sn(CH_3)_4$ preferably reacted with Rh particles (3). When $Sn(CH_3)_4$ reacted with Rh metal particles, two molecules of CH_4 per $Sn(CH_3)_4$ were evolved in the gas phase and no other hydrocarbons were observed. The samples were finally reduced with H_2 at 573 K for 1 h, followed by evacuation. By further reduction at 573 K, two more CH_4 molecules were formed, leaving no residual carbon on the surface. The reduction of the samples with H_2 at 573 K for 1 h was repeated in situ before each run. The loading of Rh was controlled to be 1.0 wt%, while the Sn/Rh ratio was varied in the range 0–1. Coimpregnation Rh–Sn/SiO_2 (denoted as Imp–Rh–Sn/SiO_2) was prepared from a methanol solution of both $RhCl_3 \cdot 3H_2O$ and $SnCl_2$. The pretreatment of these catalysts was performed in a similar way to that of Rh–Sn/SiO_2.

NO–H_2 Reaction

Catalytic NO–H_2 reactions were proceeded under $NO:H_2$ = 1.3–5.2:6.7–26.6 kPa in a closed circulating system (200 cm^3) with 0.2 g of catalyst. The reaction products were analyzed by gas chromatograph (Shimazu, GC-8A) with a 2-m column of a 5A molecular sieve and a 2-m column of Porapak R at 323 K. The reaction temperature was varied in the range of 353–393 K. H_2–D_2 exchange reaction under $NO:H_2:D_2$ = 2.7:6.7:6.7 kPa was also measured with quadrupole mass spectrometer (ULVAC MSQ-180A). The gases used in this study, NO (99.9%), H_2 (99.9999%), D_2 (99.5%), were purchased from Takachiho Co. and were used without further purification. The NO–H_2 reaction was also carried out under much lower pressure of NO ($NO:H_2$ = 2 Pa:13.3 kPa). NO pressure was estimated by mass spectrometer.

EXAFS Measurement

X-ray absorption spectra at Rh *K*- and Sn *K*-edges were measured at the BL-10B and 6B stations of the Photon Factory in the National Laboratory for High Energy Physics (Proposal No. 90003 and 92008) with a positron energy of 2.5 GeV and a maximum storage ring current of 350 mA. EXAFS data were collected in a transmission mode using ionization chambers filled with Ar for an I_0 signal and Kr for an I signal. X ray from the synchrotron radiation was monochromatized by a Si(311) channel cut crystal. The second harmonic is eliminated because of the extinction rule of Si(311), and the third and higher harmonics could be neglected to the low intensity of the photons with the corresponding energies emitted from the storage ring. The samples were treated in a closed circulating system and transferred to a glass cell with thin X-ray transparent glass windows for EXAFS spectra without contacting air. The sample under NO–H_2 reaction was prepared by evacuating the gases during the catalytic reaction, while quenching to room temperature. The EXAFS measurements were performed at either 298 or 70 K. The resulting data were analyzed by the EXAFS analysis program EXAFS2N (13). The analysis involves pre-edge extrapolation, background removal by a cubic spline method to extract EXAFS data, and Fourier transformation using a Hanning window function with one-tenth of the Fourier transform range. The typical ranges of Fourier transformation from the *k*-space to the *r*-space is 30–150 nm^{-1} for Rh *K*-edge EXAFS and 30–120 nm^{-1} for Sn *K*-edge EXAFS spectra. The inverse Fourier transformation to the *k*-space and the curve fitting were carried out to obtain detailed structural information. The detail method of the curve-fitting analysis was the same as that reported previously (3).

We used the Rh backscattering amplitude derived from Rh foil for Sn–Rh bonds because the atomic numbers of Rh and Sn are different by only 5, since no good reference compound is available for Sn–Rh bonds. In this article, curve-fitting results show the average values of Sn–Rh and Sn–Sn bondings. The phase shift function for this bonding

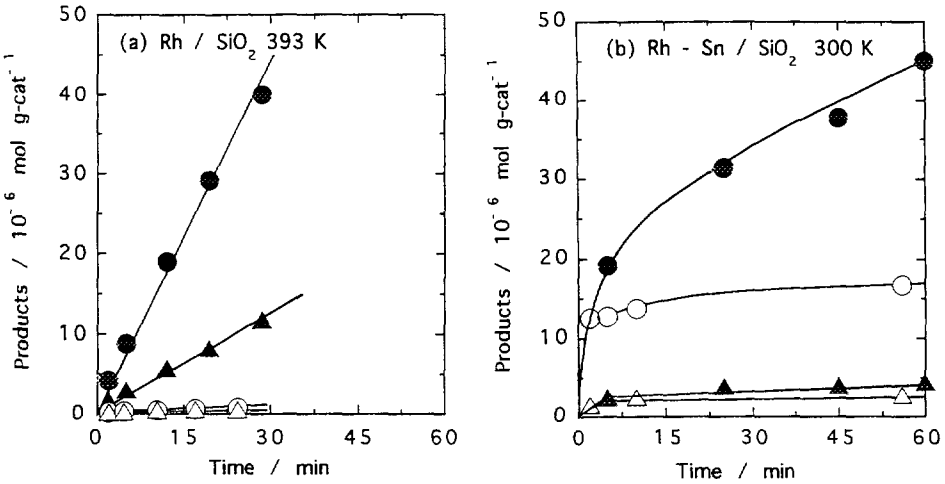

FIG. 2. The amount of products (N_2O + N_2) formed in NO decomposition and the catalytic NO–H_2 reaction on Rh/SiO_2 at 393 K (a) and on $Rh–Sn/SiO_2$ (Sn/Rh = 0.45) at 300 K (b). N_2O (●), N_2 (▲) under NO:H_2 = 2.7:13.3 kPa; N_2O (○), N_2 (△) under NO = 2.7 kPa.

was taken from the tabulated values (14). We checked the validity of this method by comparing the curve-fitting analysis by FEFF5 (15, 16) as reported before (3). In addition, we used the empirical parameters extracted from the spectra of SnO_2 and Rh foil for Sn–O and Rh–Rh bonds, respectively.

FTIR Spectra

FTIR spectra were measured on a Jasco FT–IR 7000 spectrometer in an *in situ* IR cell which was combined in a closed circulating system. The Rh/SiO_2 sample was pressed into a self-supporting disk and put into a slit of the holder in the IR cell. The reduction of Rh/SiO_2 and the subsequent reaction with $Sn(CH_3)_4$ were conducted in the IR cell under conditions similar to those mentioned above. The IR cell was designed for measuring the sample under heating or cooling by liquid N_2. IR absorption spectra were collected over 100 scans in one or a few minutes in a transmission mode and with 2 cm^{-1} resolution.

RESULTS

Profile at the Initial Stage of Reaction

Figure 2 shows the amount of the products in NO decomposition and catalytic NO–H_2 reaction as a function of reaction time. Little N_2O and N_2 were produced in NO decomposition at 383 K on Rh/SiO_2, while N_2O and N_2 increased linearly with the reaction time in NO–H_2 reaction at the same temperature (Fig. 2a). On the other hand, on $Rh–Sn/SiO_2$ (Sn/Rh = 0.45), the initial rate of the NO–H_2 reaction was much larger than the subsequent steady-state rate (Fig. 2b). When only NO was exposed to the $Rh–Sn/SiO_2$ catalyst at 300 K, N_2O and N_2 were produced very rapidly and their formation eventually stopped. By our apparatus, we were not able to measure the fast initial rate of NO decomposition on $Rh–Sn/SiO_2$ (Sn/Rh = 0.45) at 300 K. It is obvious that the addition of Sn remarkably promoted the NO dissociation on Rh/SiO_2 catalyst. The fast formation of N_2O and N_2 at the initial stage of the NO–H_2 reaction in Fig. 2b may be associated to the nearly instantaneous NO dissociation on $Rh–Sn/SiO_2$.

At the initial stage of NO dissociation on $Rh–Sn/SiO_2$ (Sn/Rh = 0.45), N_2O of ca. 1.2×10^{-5} mol/g-cat and N_2 of 0.2×10^{-5} mol/g-cat were formed, irrespective of the reaction temperature in the range 300–393 K. From this the amount of deposited oxygen atom on the catalyst can be calculated to be ca. 1.6×10^{-5} mol/g-cat. This value is close to the number of surface Rh atoms (1.5×10^{-5} mol/g-cat) and also corresponds to one-third of the number of surface Sn atoms (4.4×10^{-5} mol/g-cat) (3). NO itself was not decomposed beyond this amount of deposited oxygen atom.

Steady-State Activity

Figure 3 shows the steady-state activity of the NO–H_2 reaction at 373 K on $Rh–Sn/SiO_2$ and $Imp–Rh–Sn/SiO_2$ catalysts with various Sn/Rh composition. The catalytic activity (turnover frequency, TOF) increased with an increase of Sn added in the range of Sn/Rh $\leqq$ 0.4, showing an S-shape dependency and the activity was nearly constant in the range of Sn/Rh $\geqq$ 0.4. The highest activity of $Rh–Sn/SiO_2$ catalysts was obtained for Sn/Rh = 0.4 for which the TOF at 373 K was 75 times as high as that of a Rh/SiO_2 catalyst and 12 times as high as that of $Imp–Rh–Sn/SiO_2$ (Sn/Rh = 0.45) catalyst. The addition of Sn remarkably

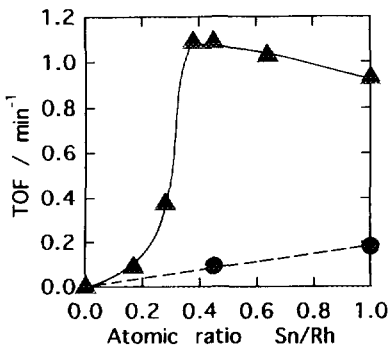

FIG. 3. The turnover frequency (produced molecules per minute per surface Rh atom) for N_2 + N_2O formation in the NO–H_2 reaction at 373 K on Rh–Sn/SiO_2 (▲) and on impregnated Rh–Sn/SiO_2 (●), NO : H_2 = 2.7 : 13.3 kPa (Rh, 1 wt%). The number of surface Rh atoms was estimated by the amount of H_2 adsorption (Rh/SiO_2) and CO adsorption (Rh–Sn/SiO_2 and Imp–Rh–Sn/SiO_2).

promoted the NO–H_2 reaction. The promoter effect was much larger with the catalysts prepared by using $Sn(CH_3)_4$ than for the Imp catalysts. The selectivity to N_2 (the ratio of N_2 to N_2 + N_2O) under the reaction condition, NO : H_2 = 2.7 kPa : 13.3 kPa was 23% on Rh/SiO_2 and 18–15% on Rh–Sn/SiO_2. NH_3 formation was negligible on both Rh/SiO_2 and Rh–Sn/SiO_2 catalysts by the analysis of mass spectrometer.

Activation Energy and Reaction Order

The activation energies for N_2O and N_2 formation in catalytic NO–H_2 reaction on Rh/SiO_2 and Rh–Sn/SiO_2 (Sn/Rh = 0.45) are listed in Table 1, where the activation energies for N_2O and N_2 formation decreased by the addition of Sn.

TABLE 1

Activation Energies and Reaction Orders for NO–H_2 Reaction on Rh/SiO_2 and Rh–Sn/SiO_2 (Sn/Rh = 0.45)

Catalysts	Products	Activation energy (kJ/mol)[a]	Reaction order[b] NO	Reaction order[b] H_2
Rh/SiO_2	N_2O	78	−0.4	0.8
	N_2	77	−0.5	0.8
Rh–Sn/SiO_2 (Sn/Rh = 0.45)	N_2O	43	0.0	0.7
	N_2	52	−0.3	0.7
	HD[c]	40	—	—

[a] Temperature range, 353–393 K; pressure, NO : H_2 = 2.7 kPa : 13.3 kPa.
[b] Reaction temperature, 393 K (Rh/SiO_2) and 373 K (Rh–Sn/SiO_2 (Sn/Rh = 0.45)); pressure range, NO : H_2 = 1.3–5.2 kPa : 6.7–26.6 kPa.
[c] Temperature range, 353–393 K; pressure, NO : H_2 : D_2 = 2.7 kPa : 6.7 kPa : 6.7 kPa.

The reaction orders with respect to NO and H_2 pressures for the NO–H_2 reaction on Rh/SiO_2 at 393 K and on Rh–Sn/SiO_2 (Sn/Rh = 0.45) at 373 K are also given in Table 1. The reaction order and activation energy for N_2O formation were similar to those for N_2 formation on Rh/SiO_2. In the case of Rh–Sn/SiO_2 (Sn/Rh = 0.45), the activation energy and the reaction order to NO pressure were different for N_2O and N_2.

Hydrogen Exchange in NO–H_2–D_2 Reaction

We continued the NO–H_2–D_2 reaction on Rh/SiO_2 and Rh–Sn/SiO_2 to examine H_2 dissociation during the catalytic NO reduction. The H_2–D_2 exchange reaction was measured under the condition of NO–H_2–D_2 (2.7 : 6.7 : 6.7 kPa) at 373 K. The rate of HD formation on Rh–Sn/SiO_2 (Sn/Rh = 0.45) was about eight times as large as that of the NO–H_2 reaction. On the other hand, on Rh/SiO_2 the H_2–D_2 exchange almost did not proceed in the range of 353–393 K.

NO–H_2 Reaction under a Very Low Pressure of NO

Figure 4 shows the NO–H_2 reaction on the Rh–Sn/SiO_2 (Sn/Rh = 0.45) catalyst at 373 K under a very low pressure of NO (NO : H_2 = 2 Pa : 13.3 kPa). Under the same condition, on Rh/SiO_2 neither N_2O nor N_2 were detected by gas chromatograph. In this condition, the TOF was much lower than that under the typical conditions (NO : H_2 = 2.7 : 13.3 kPa), but the selectivity to N_2 formation was more than 95% on Rh–Sn/SiO_2. The addition of Sn promoted both NO dissociation and selective N_2 formation at the low pressure of NO.

FTIR Measurement

Figure 5 shows *in situ* FTIR spectra on Rh/SiO_2 during the NO–H_2 reaction and under H_2 admitted after evacua-

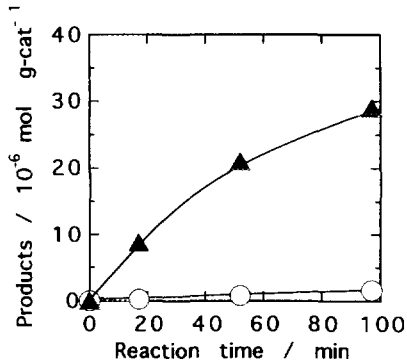

FIG. 4. The amount of products (N_2 (▲) and N_2O (○)) formed in the NO–H_2 reaction on Rh–Sn/SiO_2 (Sn/Rh = 0.45) at 373 K under NO : H_2 = 2 Pa : 13.3 kPa. The amount of products was normalized to the value per 1 g of catalyst.

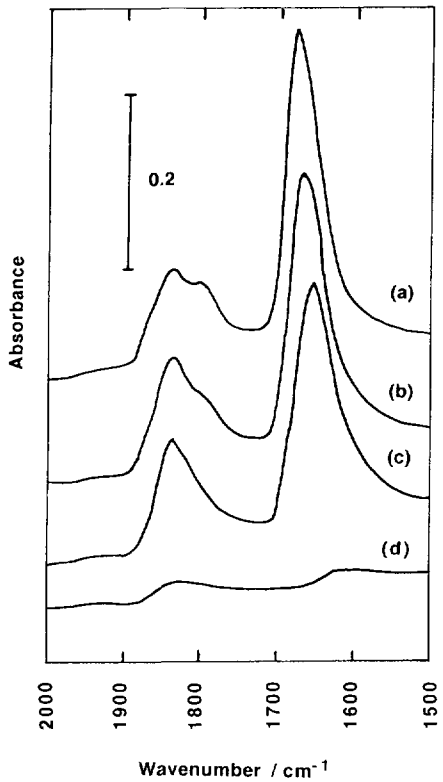

FIG. 5. FTIR spectra of NO adsorbed on the Rh/SiO_2 catalyst. (a) after the NO–H_2 (2.7 : 13.3 kPa) reaction at 373 K for 1 h; (b) 5 min after replacing the reaction gases by H_2 (13.3 kPa) at 373 K; (c) 10 min after replacing the reaction gases by H_2 (13.3 kPa) at 373 K; (d) 30 min after replacing the reaction gases by H_2 (13.3 kPa) at 373 K.

tion of the reactant gases. The spectra were taken at 373 K and NO : H_2 = 2.7 : 13.3 kPa. Three peaks at 1830, 1796, and 1680 cm^{-1} for adsorbed NO were observed during the NO–H_2 reaction. The peak of 1680 cm^{-1} may be referred to two-fold bridge NO species and the peaks at 1830 and 1796 cm^{-1} are assigned to linear NO species similarly to HREELS studies on NO/Rh(111) (17, 18). NO molecules seem to adsorb preferably on two-fold bridge sites of the surface of Rh metal particles supported on SiO_2 rather than on top sites because of the larger intensity of the 1680 cm^{-1} peak than two others at 1830 and 1796 cm^{-1}. Similar results have been observed on the Rh(111) surface (17, 18). No band was observed around 1910 cm^{-1} which has been referred to as $Rh–NO^{\delta+}$ (19). When a mixture of NO and H_2 was replaced by H_2 during the NO–H_2 reaction, these peaks decreased very slowly till 10 min after H_2 introduction as shown in Fig. 5. Then, the peaks decreased more rapidly by the reaction with H_2. From the similar experiments on the Rh/SiO_2 catalyst by gas chromatograph, the initial decrease of the peaks corresponded to the catalytic reaction rate for the NO–H_2 reaction. The higher reaction rate in the adsorbed NO–H_2 reaction after ca. 10 min is compatible with the reaction order of −0.4 or −0.5 with respect to NO pressure.

Figure 6 shows *in situ* FTIR spectra on $Rh–Sn/SiO_2$ (Sn/Rh = 0.45) during the NO–H_2 reaction and under H_2 admitted after evacuation of the reactant gases. The spectra were taken at 343 K under NO : H_2 = 2.7 : 13.3 kPa. Two peaks at 1809 and 1635 cm^{-1} were observed. The 1809 cm^{-1} peak is attributed to linear NO species adsorbed on Rh atoms. When the reaction gases (NO + H_2) was replaced by H_2, two peaks decreased, corresponding to the steady-state rate of the NO–H_2 reaction on $Rh–Sn/SiO_2$ at this temperature. The 1635 cm^{-1} peak might be attributed to two-fold bridge NO, but this is unlikely from the surface geometry in Fig. 1. The 1635 cm^{-1} peak disappeared faster than the 1809 cm^{-1} peak as shown in Fig. 6.

Figure 7 shows FTIR spectra on $Rh–Sn/SiO_2$ (Sn/Rh = 0.45) under NO of 2.7 kPa at three different temperatures. While only linear NO species was observed at 150 K, by heating to 250 K, the lower frequency peak appeared. In this stage, N_2O (main) and N_2 (minor) were produced. The larger the amount of N_2O + N_2 formed by heating to the higher temperature (Figs. 7b–7c), the larger the intensity of the 1635 cm^{-1} peak became. Note that the spectra of adsorbed NO on $Rh–Sn/SiO_2$ are different at 348 K (Fig. 6a) and 150 K (Fig. 7a).

EXAFS Measurement

Figure 8 shows the Sn *K*-edge EXAFS oscillations for $Rh–Sn/SiO_2$ (Sn/Rh = 0.45) after H_2 reduction at 573 K,

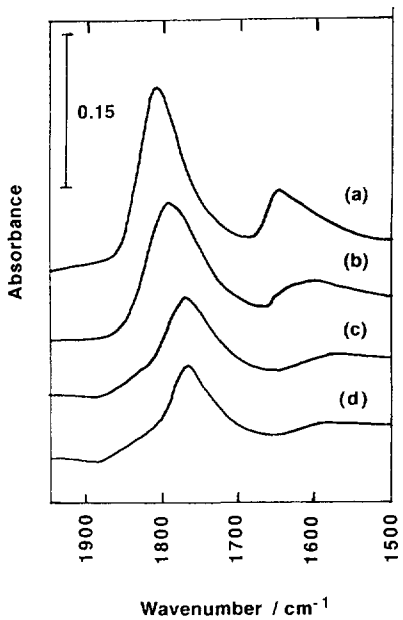

FIG. 6. FTIR spectra of NO adsorbed on $Rh–Sn/SiO_2$ (Sn/Rh = 0.45). (a) after NO–H_2 (2.7 : 13.3 kPa) reaction at 348 K for 1 h; (b) 1 min after replacing the reaction gases by H_2 (13.3 kPa) at 348 K; (c) 2 min after replacing the reaction gases by H_2 (13.3 kPa) at 348 K; (d) 3 min after replacing the reaction gases by H_2 (13.3 kPa) at 348 K.

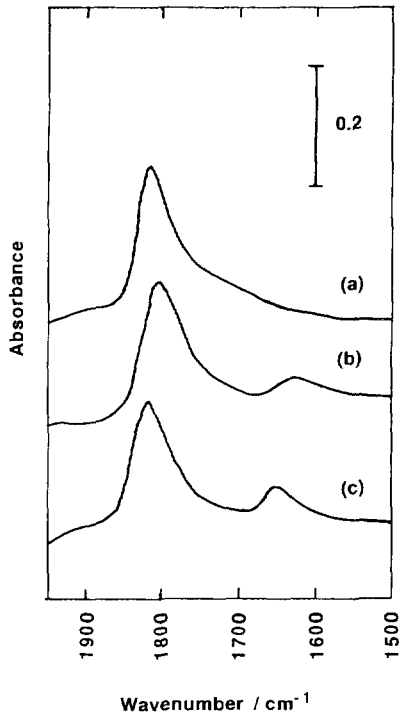

FIG. 7. FTIR spectra of NO adsorbed on Rh-Sn/SiO_2 (Sn/Rh = 0.45) under NO of 2.7 kPa at different temperatures. (a) 150 K, (b) 250 K, (c) 298 K.

during NO-H_2 reaction at 373 K and after heating the sample to 573 K after evacuation. These EXAFS spectra were taken successively in a series of experiments to examine a change of surface species. We have reported the results of curve-fitting analysis of Sn *K*-edge EXAFS spectra for Rh-Sn/SiO_2 (Sn/Rh = 0.45) after H_2 reduction as shown in Table 2 and Fig. 1 (2, 3). Observation of Sn-Rh or -Sn bonds without contribution to the Sn-O bond on the reduced catalyst coincides with the EXAFS analysis by Meitzner *et al.* (20). The Fourier transforms associated with the EXAFS oscillations are shown in Fig. 9. The Fourier transform in Fig. 9a has been referred to as Sn-Rh or -Sn bonds. There is also a small peak for the reduced catalyst at a position similar to the second peak in Fig. 9a. However, the second peak intensity in Fig. 9b is much larger than that in Fig. 9a. For the catalyst exposed to a mixture of NO and H_2 at 373 K, two other peaks at ca. 0.15 nm and 0.20 nm (phase shift, uncorrected) appeared, while Sn-Rh or -Sn bonds remained almost unchanged. When the reaction gases were evacuated at 373 K and the sample was heated to 573 K under vacuum, the intensity of the 0.15-nm peak (phase shift, uncorrected) increased whereas the 0.20-nm peak (phase shift, uncorrected) almost disappeared. The peak of Sn-Rh or -Sn bonds reduced a little. By this treatment, adsorbed NO species all desorbed as N_2 and N_2O by the gas-phase analysis and by FTIR measurement, which indicates that oxygen atoms were left on the surface. The change of oscillation in Figs. 8a-8c particularly in the lower wavenumber region may be due to the contribution of light element like oxygen in this system, coinciding with the FTIR data and the reaction stoichiometry. The first peak of the Fourier transforms b and c is straightforwardly assigned to the Sn-O bond. The second peak of the Fourier transform b was observed by EXAFS only when molecularly adsorbed NO species was observed by FTIR. Therefore, it is most likely that this peak is attributable to the Sn-O bond. The curve-fitting analysis is shown in Fig. 10, by assuming two Sn-O bond in addition to the Sn-metal bonds. The number (N_i) of the independent parameters in the curve-fitting analysis

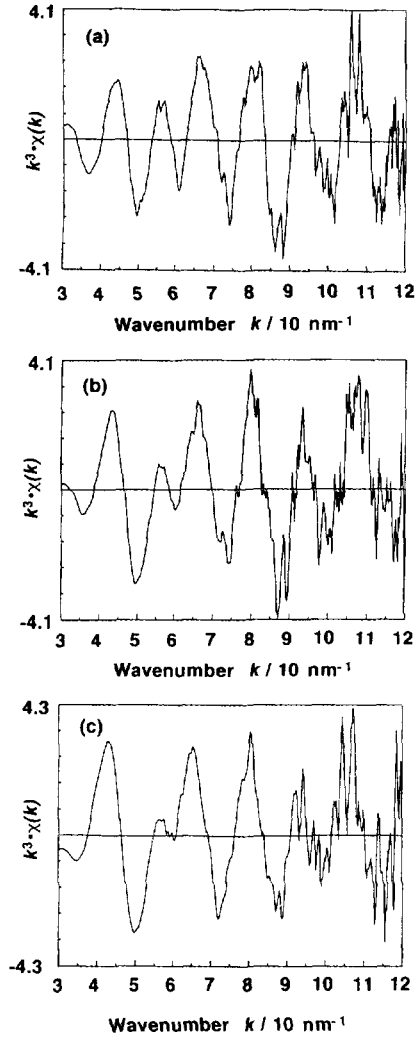

FIG. 8. Sn *K*-edge EXAFS oscillations for Rh-Sn/SiO_2 (Sn/Rh = 0.45). (a) k^3-weighted $\chi(k)$ of the sample after H_2 reduction at 573 K; (b) k^3-weighted $\chi(k)$ of the sample during NO-H_2 (2.7 : 13.3 kPa) reaction at 373 K; (c) k^3-weighted $\chi(k)$ of the sample after heating (b) to 573 K under vacuum.

TABLE 2

The Curve-Fitting Results for Sn *K*-Edge EXAFS Spectra of Rh–Sn/SiO_2 (Sn/Rh = 0.45) after the H_2 Reduction and under NO–H_2 Reaction at 373 K

	Backscattering atom	CN[a]	R (nm)[b]	ΔE_0 (eV)[c]	σ (nm)[d]	R_f (%)[e]
After H_2 reduction	Sn or Rh	5.9 ± 2.4	0.270 ± 0.002	4.4 ± 4.0	0.0109 ± 0.0016	4.0
	Sn or Rh	2.6 ± 1.0	0.290 ± 0.002	6.3 ± 4.0	0.0114 ± 0.0016	
NO–H_2 reaction	O	1.0 ± 0.2	0.205 ± 0.002	−0.6 ± 4.0	0.0070 ± 0.0010	2.0
	O	0.4 ± 0.2	0.256 ± 0.002	0.0 ± 4.0	0.0070 ± 0.0016	
	Sn or Rh	5.7 ± 2.4	0.269 ± 0.002	2.9 ± 4.0	0.0109 ± 0.0016	
	Sn or Rh	3.1 ± 1.0	0.286 ± 0.002	2.1 ± 4.0	0.0119 ± 0.0016	

[a] Coordination number.
[b] Bond distance.
[c] The difference between origins of photoelectron wave vector.
[d] Debye-Waller factor.
[e] R factor; the definition of R factor and the estimation of error bars are found in Ref. (3).

Note. Fourier transform range, 30–120 nm^{-1}; Fourier filtering range (0.10–0.32 nm); curve-fitting parameters for Sn–Rh or –Sn bonds; theoretical phase shift function and empirical amplitude parameter extracted from the spectra of Rh metal (CN = 12, R = 0.268 nm, σ = 0.0060 nm, ΔE_0 = 0.0 eV); curve-fitting parameters for Sn–O bonds, empirical phase shift and amplitude functions extracted from SnO_2 (CN = 6, R = 0.205 nm, σ = 0.0060 nm, ΔE_0 = 0.0 eV).

is limited by the formula described by Stern (21); $N_I = (2\,\Delta k\,\Delta R/\pi) + 2$ (where Δk is the Fourier transform range and ΔR is the Fourier filtering range). In our case (Δk = 9.0, ΔR = 2.2), N_I is calculated to be 14.6. Because there are four fitting parameters (CN, R, ΔE_0, σ) for each bond, we can proceed curve fitting by three kinds of bonds. For the catalyst exposed to NO + H_2, the three bonds correspond to Sn–O, Sn–O, and Sn–Rh (–Sn). The three-peak analysis is compatible with the definite separation among these peak positions. In addition, we assumed a similar structure in the bimetallic layers of the reduced catalyst involving a long Sn–Rh (–Sn) contribution (3). In fact, the CN, R, ΔE_0, σ values for Sn–O and Sn–O were fixed at the values determined by the three-shell fitting. Then, the four-shell fitting (Sn–O, Sn–O, Sn–Rh [–Sn] and Sn–Rh [–Sn]) was performed. The fitting values for Sn–Rh (–Sn) bonds were very close to those for the reduced catalyst (Table 2). The best fit result is given in Table 2. The Sn–O bond distances were determined to be 0.205 and 0.256 nm.

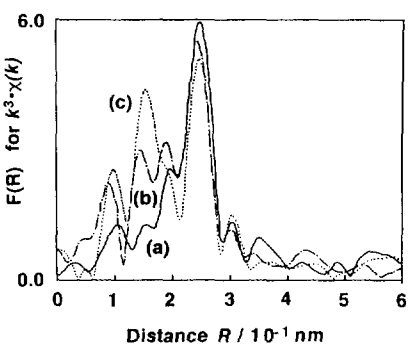

FIG. 9. Fourier transforms associated with Figs. 8a–8c, respectively. Fourier transform range, 30–120 nm^{-1}.

When the sample of Fig. 9b was exposed to H_2 (13.3 kPa) at 373 K, both Sn–O bonds disappeared and only Sn–Rh or –Sn bonds were observed, reproducing Fig. 9a.

The Rh *K*-edge EXAFS spectra for Rh–Sn/SiO_2 (Sn/Rh = 0.45) exposed to NO + H_2 were almost the same as that after H_2 reduction reported previously (3). This is due to a low population of surface Rh atoms (Rhs/Rh = 0.14).

DISCUSSION

Promoter Effects of Sn for NO–H_2 Reaction on Rh–Sn/SiO_2

The rate-determining step for the catalytic NO–H_2 reaction on Rh/SiO_2 has been proposed to be a hydrogen-assisted NO dissociation (10):

$$NO_{(a)} + H_{(a)} \rightarrow N_{(a)} + OH_{(a)}. \qquad [1]$$

The activation energy determined in the present study on Rh/SiO_2 (Table 1) is similar to that in the literature (10). The feature of the catalytic NO–H_2 reaction, which is enhanced by the presence of H_2 as compared to the decomposition of NO alone on Rh/SiO_2, was observed in Fig. 2. These results are compatible with the proposed mechanism, involving a slow step (Eq. [1]) (10). The negative reaction orders to NO pressure in Table 1 suggest that H_2

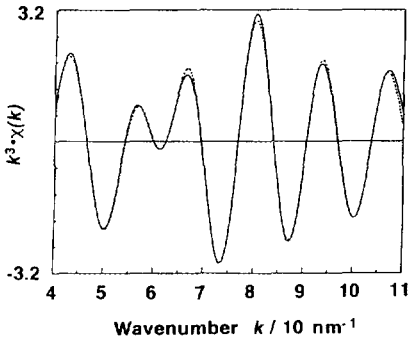

FIG. 10. Curve-fitting analysis for the sample (b) in Fig. 8 by four waves (Sn–O + Sn–O + Sn–Rh or –Sn + Sn–Rh or –Sn). Solid line, observed; dotted line, calculated. Measurement temperature, room temperature; Fourier transform range, 30–120 nm^{-1}; Fourier filtering range, 0.10–0.32 nm.

dissociation on the vacant Rh sites is more important for catalytic NO–H_2 reaction because of a strong block of the sites by NO on Rh/SiO_2.

The most characteristic feature of the Rh–Sn/SiO_2 catalyst unlike the Rh/SiO_2 catalyst is ready NO dissociation without aid of adsorbed hydrogen atoms. NO dissociation to form N_2O and N_2 on Rh–Sn/SiO_2 occurred at a temperature as low as 200 K. NO dissociation almost instantaneously proceeded, followed by a steady-state reaction in the presence of H_2 as shown in Fig. 2b. It is very unlikely that NO dissociation is the rate-determining step on Rh–Sn/SiO_2. The rate-determining step seems to be H_2 dissociation or the reduction of surface oxygen atoms produced by NO dissociation. On Rh–Sn/SiO_2 catalysts, the rate of the H–D exchange reaction in NO–H_2–D_2 reaction at 373 K was about eight times higher than that of N_2O + N_2 of the steady-state NO–H_2 reaction. The activation energy (40 kJ/mol) for the H–D exchange reaction is slightly lower than the activation energy (43 and 52 kJ/mol) of the catalytic NO–H_2 reaction. Thus, the removal of the surface oxygen atoms by hydrogen rather than the dissociation step of the hydrogen molecule may control the steady-state rate. In fact, the peak intensity of the Sn–O bond at 0.205 nm in the Fourier transform for the catalyst under catalytic reaction conditions at 373 K was about three-fourths of that observed by the dissociation of NO alone at 373 K. The oxygen affinity of H_2 is larger than that of Sn, which demonstrates that SnO_x can be reduced with H_2 (4). On Rh–Sn/SiO_2 catalysts, the NO dissociation reaction was drastically promoted by the addition of Sn; the rate-determining step is not the NO dissociation but the reduction of surface oxygen (Sn–O : 0.205 nm) by hydrogen.

One of promoting effects of Sn in NO dissociation is caused by the oxygen affinity of Sn to form Sn–O bonds. But the increase of the catalytic activity is not proportional to the amount of Sn added as shown in Fig. 3. At low Sn/Rh ratio, the activity increase is weak. It becomes drastically abrupt at Sn/Rh = 0.3 until reaching the saturation value at Sn/Rh = 0.4 as a function of Sn quantity. It has been demonstrated that Rh–Sn/SiO_2 with Sn/Rh = 0.45 has the surface composition of Sn_s/Rh_s = 3, where surface Rh atoms are isolated and surrounded by six Sn atoms as shown in Fig. 1 (1, 3). The bimetallic ensemble structure provides easy dissociation of NO to form Sn–O bonds at 0.205 nm with the saturation coverage of $O_{(a)}$ being one-third of the surface Sn atoms, which is compatible with the model that the $O_{(a)}$ is located at the three-fold hollow sites of Sn_3 ensembles.

Observation of the Reaction Intermediate of NO–H_2 Reaction on Rh–Sn/SiO_2 Catalyst

Two kinds of adsorbed NO species on Rh–Sn/SiO_2 during the NO–H_2 reaction were observed by FTIR in Fig. 6. Judging from the frequency of peaks, the higher frequency peak (1809 cm^{-1}) is attributed to linear NO species adsorbed on Rh atom because NO does not adsorb on Sn metal. The lower frequency peak (1635 cm^{-1}) can possibly be assigned to two-fold bridge NO or bent NO species. The Rh atoms on the Rh–Sn/SiO_2 with Sn_s/Rh_s = 3 are distributed as the isolated atoms at the bimetallic surface in Fig. 1 (2, 3). In fact, in the case of CO adsorption no bridge CO was observed by FTIR. If the 1635-cm^{-1} peak was due to a two-fold bridge NO species and when NO is adsorbed on Rh–Sn/SiO_2 at 150 K, the bridge NO peak should have appeared because NO molecules on Rh metal adsorb on two-fold bridge sites more favorably than on top sites (17, 18) (Fig. 5). Actually, only one peak was observed in Fig. 7. Thus, the 1635 cm^{-1} peak may be assigned to a bent-type NO species. This is compatible with the EXAFS analysis under conditions similar to those of the FTIR measurements.

In Fig. 9b of Sn *K*-edge EXAFS two peaks at 0.15 and 0.20 nm (phase shift, uncorrected) were observed during the NO–H_2 reaction at 373 K. Exposure of Rh–Sn/SiO_2 to O_2 at room temperature showed a similar peak to the first peak in the Fourier transform of Sn *K*-edge EXAFS. Therefore the first peak is straightforwardly assigned to the Sn–O bond. The second peak disappeared by evacuation at 573 K after the NO–H_2 reaction at 373 K (Fig. 9c). At the same time, the NO peak disappeared, evolving N_2 (main) and N_2O (minor) and leaving O atoms at the catalyst surfaces. The O atoms make the bonds with Sn atoms, which coincides with the increase in the intensity of the peak at 0.15 nm in Figs. 9b–9c. The behavior of adsorbed NO species in FTIR and TPD spectra also coincides with the disappearance of the second peak in the EXAFS Fourier transform (Fig. 9). These results suggest that the lower-frequency peak in Fig. 6 and the second peak of the Fourier

transform in Fig. 9 are assigned to a bent-type NO species interacting with Sn atoms. The 1635 cm^{-1} peak appeared on the partially oxidized surface as shown in Fig. 7, where N_2 and N_2O were evolved by heating to 250 K after adsorption of NO at 150 K, indicating the partial oxidation of the surface by NO dissociation. No nitrogen oxide molecule dissociates on Rh–Sn/SiO_2 at 150 K. The oxygen atom of the bent-type NO molecule adsorbed on the partially oxidized surface seems to create the Sn–O bond by ionic interaction between NO and $Sn^{\delta+}$ (12). From all the data, finally we carefully performed the detailed EXAFS analysis by assuming two oxygen bonds (Sn–O + Sn–O) in addition to the Sn–Rh or –Sn bonds at 0.270 and 0.290 nm (3). The best fit result is shown in Fig. 10 and the bond distances and coordination numbers of Sn–O and other EXAFS parameters are listed in Table 2. The Sn–O bond length of 0.205 nm is close to that expected for SnO_2 (0.206 nm). The longer Sn–O bond distance was determined to be 0.256 nm. The Sn–O (N) bonding may be a main factor for NO tilting, and the bond length of 0.256 nm leads to the bent orientation with the molecular axis nearly parallel to the surface.

The adsorbed NO reacts with H_2 at 373 K, but the bent NO disappears more rapidly than the linear NO as shown in Fig. 6. The reason is not clear at present, but in the absence of NO in the gas phase the linear NO species adsorbed on an isolated Rh atom may not move as rapidly to a vacant Rh atom where the bent NO is consumed by dissociation by a geometric factor. Under the catalytic reaction conditions, NO can be supplied to adsorb everywhere at the bimetallic ensemble surface.

Reaction Mechanism for Catalytic NO–H_2 Reaction on Rh–Sn/SiO_2 Catalysts

Figure 11 shows a scheme of the reaction mechanism for catalytic NO–H_2 reaction on Rh–Sn/SiO_2 (Sn/Rh = 0.45). In this scheme, the Rh–Sn bimetallic ensemble structure is based on the characterization of reduced Rh–Sn/SiO_2 catalysts by means of Sn *K*- and Rh *K*-edge EXAFS, FTIR, TEM, CO, and H_2 adsorption (2, 3).

NO dissociation to nitrogen and oxygen atoms on Rh–Sn/SiO_2 occurs even at 200 K. At 373 K it is almost instantaneous. From Sn *K*-edge EXAFS analysis, the oxygen atom adsorbs on the surface Sn atoms, showing Sn–O bond at 0.205 nm, and its coordination number is about one (Table 2). The coverage of the oxygen atom is one-third of the amount of the surface Sn atoms. From these results, oxygen atoms are proposed to be located on the three-fold sites consisting of three Sn atoms. The nitrogen atom produced on the Rh atom mainly reacts with NO to form N_2O. The adsorbed NO species is of linear type (1809 cm^{-1}) or of bent type (1635 cm^{-1}), the latter species interacting with the $Sn^{\delta+}$ atom (Sn–O = 0.256 nm), which is partially oxidized by the adsorbed O atoms (Fig. 11e). Due

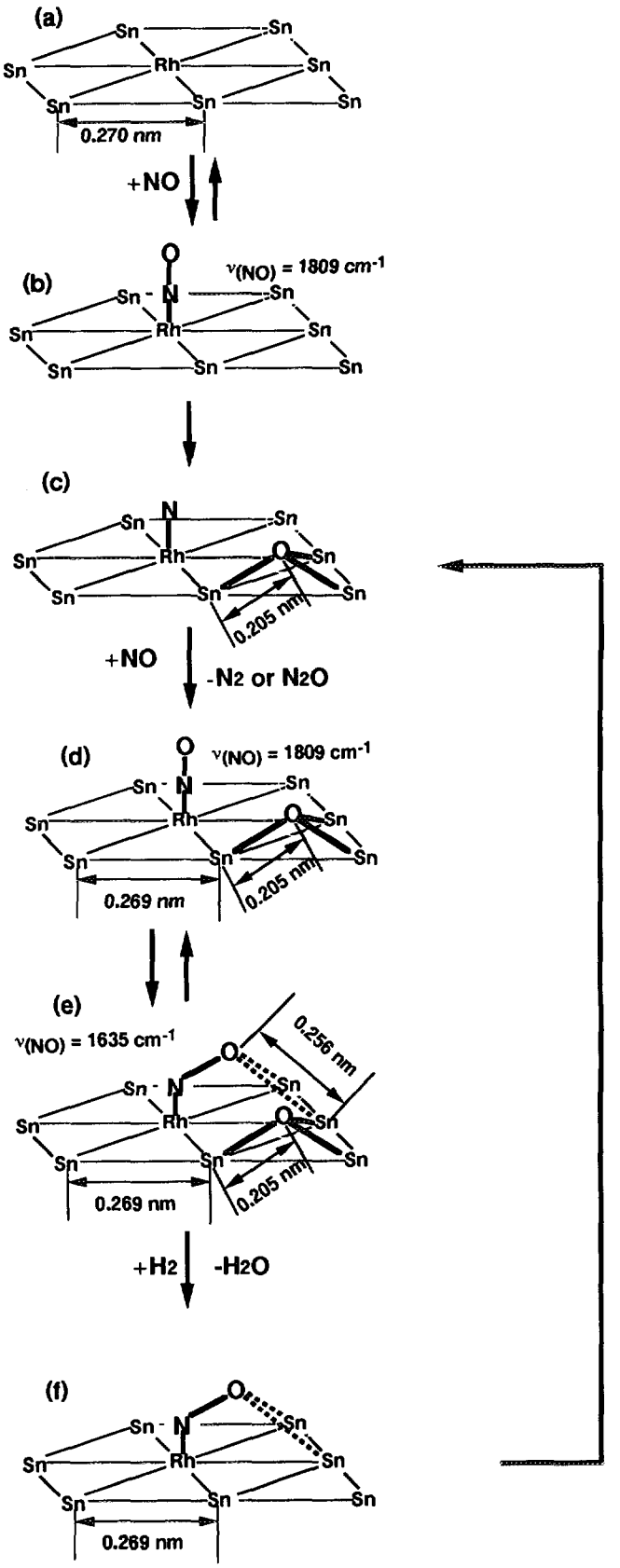

FIG. 11. A reaction mechanism for the catalytic NO–H_2 reaction on Rh–Sn/SiO_2.

to geometric reasons and the fact that the longer bond between the molecular species and the surface atoms was observed by EXAFS as a definite peak in the Fourier transform (Fig. 9b), we propose that the oxygen atom of the NO molecule makes chemical bonds with two $Sn^{\delta+}$ atoms.

We have no molecular information on the H_2 dissociation sites. The rate of the H_2–D_2 exchange reaction during the NO–H_2–D_2 reaction on Rh–Sn/SiO_2 was much faster than the rate of N_2O + N_2 formation, which is contrasted to the slow H_2–D_2 exchange in the NO–H_2–D_2 reaction on Rh/SiO_2. These results imply the contribution of SnO_x sites to H_2 dissociation. But the usual Sn oxides are known to be relatively inactive at 373 K. Therefore, H_2 may dissociate heterolytically on Rh and $O(Sn)_3$ sites. The stretching vibration of H–OSn was not observed, probably because the concentration of this species was so small under the reaction conditions. This step (Figs. 11e–11f) is the rate-determining step for the catalytic NO–H_2 reaction on Rh–Sn/SiO_2 (Sn/Rh = 0.45).

Under very low pressure of NO, N_2 was produced as a main product in Fig. 4. Under this condition the catalyst surface can keep the metallic state. The $N_{(a)}$ atoms may be recombined to N_2 or react with NO to form N_2O, which is also decomposed to N_2 on the bimetallic surface.

CONCLUSIONS

1. The Rh–Sn/SiO_2 catalyst highly active for the NO dissociation and the catalytic NO–H_2 reaction under mild conditions was prepared by selective reaction between Rh particles on SiO_2 and $Sn(CH_3)_4$ vapor.

2. The FTIR spectra of adsorbed NO at low temperatures and at reaction temperatures suggested the presence of active bent NO species.

3. The molecular reaction intermediate, bent NO species, was observed by EXAFS.

4. The different kinetic parameters on Rh/SiO_2 and Rh–Sn/SiO_2 reflect the different reaction mechanism for the NO–H_2 reaction.

5. A reaction mechanism was discussed on the basis of the active ensemble structure with a surface composition of Sn_s/Rh_s = 3.

REFERENCES

1. Tomishige, K., Asakura, K., and Iwasawa, Y., *J. Chem. Soc., Chem. Commun.*, 184 (1993).
2. Tomishige, K., Asakura, K., and Iwasawa, Y., *Catal. Lett.* **20,** 15 (1993).
3. Tomishige, K., Asakura, K., and Iwasawa, Y., *J. Catal.* **149,** 70 (1994).
4. Reed, T. B., *in* "Free Energy of Formation of Binary Compounds," p. 67. MIT Press, Cambridge, MA 1971.
5. Nishiyama, S., Akemoto, M., Yamamoto, I., Tsuruya, S., and Masai, M., *J. Chem. Soc. Faraday Trans.* **88,** 3483 (1992).
6. Candy, J. P., Mansour, A. E., Ferretti, O. A., Mabilon, G., Bournonville, J. P., Basset, J. M., and Martino, G., *J. Catal.* **112,** 201 (1988).
7. Candy, J. P., Ferretti, O. A., Mabilon, G., Bournonville, J. P., Mansour, A. E., Basset, J. M., and Martino, G., *J. Catal.* **112,** 210 (1988).
8. Agnelli, M., Candy, J. P., Basset, J. M., Bournonville, J. P., and Ferretti, O. A., *J. Catal.* **121,** 236 (1990).
9. Basset, J. M., Candy, J. P., Louessard, P., Ferretti, O. A., and Bournonville, J. P., *Wiss. Z. Tech. Hochsch. Leuna-Merseburg* **32,** 657 (1990).
10. Hecker, W. C., and Bell, A. T., *J. Catal.* **92,** 247 (1985).
11. Hecker, W. C., and Bell, A. T., *J. Catal.* **84,** 200 (1983).
12. Tomishige, K., Asakura, K., and Iwasawa, Y., *Chem. Lett.*, 235 (1994).
13. Kosugi, N., and Kuroda, H., "Program EXAFS2N." University of Tokyo, 1987.
14. Teo, B. K., and Lee, P. A., *J. Am. Chem. Soc.* **101,** 2815 (1979).
15. Rehr, J. J., Leon, J. M., Zabinsky, S. I., and Albers, R. C., *J. Am. Chem. Soc.* **113,** 5135 (1991).
16. Leon, J. M., Rehr, J. J., Zabinsky, S. I., and Albers, R. C., *Phys. Rev. B* **44,** 4146 (1991).
17. Root, T. W., Fisher, G. B., and Schmidt, L. D., *J. Chem. Phys.* **85,** 4679 (1986).
18. Root, T. W., Fisher, G. B., and Schmidt, L. D., *J. Chem. Phys.* **85,** 4687 (1986).
19. Arai, H., and Tominaga, H., *J. Catal.* **43,** 131 (1976).
20. Meitzner, G., Via, G. H., Lytle, F. W., Fung, S. C., and Sinfelt, J. H., *J. Phys. Chem.* **92,** 2925, (1988).
21. Stern, E. A., *Phys. Rev. B* **48,** 9825 (1993).